INORGANIC CHEMISTRY
FRONTIERS

REVIEW

View Article Online
View Journal | View Issue

Cite this: *Inorg. Chem. Front.*, 2020, **7**, 12

Alterations to secondary building units of metal–organic frameworks for the development of new functions

Junsu Ha, Jae Hwa Lee * and Hoi Ri Moon *

Secondary building units (SBUs) are the key components of metal–organic frameworks (MOFs) that help to build potentially porous periodic networks by linking multitopic organic ligands. Hence, metal SBUs are critical for determining the underlying topology of MOFs. Moreover, SBUs are the main MOF research topic nowadays, because of the simplicity of their synthesis, diverse directionality and their ability to easily harness open metal sites, compared to that of primary building units (comprising mononuclear metal centres) or tertiary building units (metal–organic polyhedra). Therefore, post-synthetic approaches for altering SBUs do not only include developing techniques for controlling the properties of MOFs but also involve a more in-depth understanding of their structure–function relationships from the materials science and engineering perspective. The SBU-related reviews published to date have successfully introduced and organised the chemistry of SBUs in MOFs. Because many recent studies have explored more diverse methods, such as metal exchange, oxidation-state transformation, defect generation, and incorporation of other species, in this review, we mainly focus on the recently developed methods for SBU alteration by classifying them into four groups and elaborate on how unique structures and properties can be achieved using those methods.

Received 31st August 2019,
Accepted 26th October 2019

DOI: 10.1039/c9qi01119f

rsc.li/frontiers-inorganic

1. Introduction

Metal–organic frameworks (MOFs) are the most prominent class of reticular compounds that link molecular building blocks (organic and inorganic) *via* coordinating bonds into periodic structures that contain potential voids.[1–3] The pro-

Department of Chemistry, Ulsan National Institute of Science and Technology (UNIST), 50 UNIST-gil, Ulsan 44919, Republic of Korea.
E-mail: hoirimoon@unist.ac.kr

Junsu Ha

Junsu Ha received his bachelor's degree in chemistry from Inha University, Korea, in 2018. He is currently pursuing a combined MS-PhD program at Ulsan National Institute of Science and Technology (UNIST) under the supervision of Prof. Hoi Ri Moon. His research interests are the development of MOFs for molecular separation and the design of MOF heterostructures.

Jae Hwa Lee

Jae Hwa Lee received his BS in 2013 from Interdisciplinary Green Energy, Ulsan National Institute of Science and Technology (UNIST), and PhD in 2019 from the Department of Chemistry, UNIST. Currently, he is working as a postdoctoral fellow at UNIST with Prof. Hoi Ri Moon, supported by National Research Foundation of Korea (NRF) and Samsung Research Funding & Incubation Centre of Samsung Electronics. His research focuses on the synthesis of metal–organic frameworks and their crystal engineering for gas storage, separation, molecular sensing, and catalytic reaction.

perties and structures of MOFs have recently attracted the attention of scientists; moreover, they have been the subject of thousands of papers annually, owing to their modular topology, chemical variety, and controllable morphology, which are attributed to the combination of their organic and inorganic characteristics.[4,5] In describing MOF structures, secondary building units (SBUs) designate clusters of metal (M) ions joined to more than one other metal *via* non-metal bonds (*e.g.*, M–O–M and M–O–C–O–M; oxo and carboxylate bonds, respectively) that form 3D periodic networks.[6] Therefore, the development of novel SBUs is essential for the advancement of the topological directionality of MOFs and the achievement of stable MOFs.

In the late 1980s and 1990s, many researchers focused on assemblies of single metal ions and neutral donor linkers to construct coordination networks that could accommodate guest solvent molecules in their pores.[7–11] However, most compounds irreversibly collapsed upon removing the guest molecules owing to their structural fragility which was attributed to the resultant coordination geometries based on single metals. Therefore, the discovery and use of polynuclear inorganic clusters (*i.e.*, SBUs) has conferred thermodynamically and mechanically stable coordination environments, owing to the entanglement of SBUs *via* chelation and the bridging of multidentate ligands, such as carboxylate and phosphate. MOF-5, a representative MOF comprising octahedral SBUs of Zn_4O tetrahedra, is regarded as a rigid and stable framework because the six extension point SBU restricts the movement of the linker and secures the position of the metal centres.[12–14] Accordingly, flexible frameworks should be ascribed to SBUs that exhibit sufficiently strong coordination to preserve structural integrity yet allow hinge movements with certain degree of freedom.[14,15] Based on the hard and soft acid and base (HSAB) theory, hard Lewis acids (Fe^{3+}, Cr^{3+}, Zr^{4+}, and Ti^{4+}) could react with hard Lewis bases (carboxyl-based ligands) to obtain hydrolytically and chemically ultra-stable MOFs.[16–19]

Hoi Ri Moon

Hoi Ri Moon received her BS in 2001 from Ewha Womans University and PhD in 2007 from Seoul National University. After working as a postdoctoral fellow at Molecular Foundry, Lawrence Berkeley National Laboratory, she joined Ulsan National Institute of Science and Technology (UNIST) in 2010 as an assistant professor and was promoted to an associate professor in 2014. Her group aims to understand the flexible behaviours of metal–organic frameworks (MOFs) and create unique MOFs for gas separation (especially hydrogen isotope separation), gas storage, molecular sensing and heterogeneous catalysis.

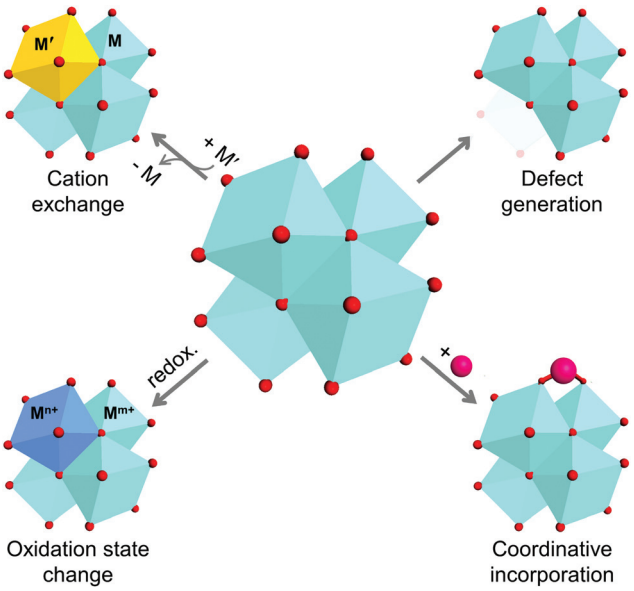

Scheme 1 Schematic illustration of four methods for alteration of secondary building units of metal–organic frameworks.

As previously described, metal ions/clusters and organic ligands are the two main parts of MOF structures, and are commonly considered to be the 'joints' and 'struts' of such structures. The direct assembly of the joints and struts dictates the structure and physicochemical properties of the MOF, and could limit the extent of their tunability. Thus, the concept of post-synthetic modification (PSM) emerged owing to the need of chemists and engineers to control the functions and expand the capability of MOFs. The initial studies on the PSM of MOFs were conducted in 1999 and became mainstream by 2007.[12,20] However, because the introduction of versatile functional groups to organic linkers is more eidetic and straightforward compared to that of inorganic components, many previous reviews have focused more on the chemical alteration of ligands. The relevant PSM methods for the inorganic clusters in MOFs can be classified as: (1) substitution of cations, (2) variation of cation valence, (3) generation of vacancies, and (4) incorporation of new species (Scheme 1). These methods are also regarded as rational tools for modulating the properties of conventional inorganic solids, including minerals, nanocrystals, and organometallic complexes.[21–29]

The SBU term should be differentiated from the 'metal node' one in certain cases; for example, single metal ions, such as those present in zeolitic imidazolate frameworks, could be designated as single-metal nodes or primary building units.[11,30] In addition, neither the metal complexes located within the pores nor the metalloligands (ligands that contain metals) are considered to be SBUs. Hence, this review is limited to the chemical and/or mechanical alteration of SBUs. The PSM of SBUs has already generated many novel MOFs that could not have otherwise been obtained, and that present great potential for diverse applications. More specific reviews for each PSM method have been already published;[31–35]

however, broad terms comprehensive report has been scarcely published to date. For example, the previous reviews published by Wang *et al.*[12] and Cohen *et al.*[20] described the general concept of PSM for MOFs, but mainly focused on the covalent PSM of organic linkers, while the PSM of metal SBUs was only partially described. While several reviews addressed SBU alteration methods and results in detail, they only focused on one method each: the 2014 report published by Dincă *et al.*[36] described the cation exchange alteration method and the 2015 and 2018 reports authored by Fischer *et al.*[37,38] addressed defective engineering. Therefore, this review is intended to briefly introduce the general PSM strategies for SBUs and conceptualise them, to offer a toolbox that MOF researchers could use to design and engineer novel MOFs in a more systematic and versatile way.

2. Strategies for SBU alteration

2.1 Cation exchange at SBUs

Cation exchange of the SBUs is defined as a partial or complete substitution of a metal ion for another while retaining the framework[34] and has been utilised by the MOF chemists to alter the inherent properties derived from metal clusters such as adsorption enthalpies and catalytic activities. The process usually involves mild and gradual reaction in a solution of the target cation. Dincă and Long, for the first time in 2007, performed a series of cation exchange experiments to vary the H_2 adsorption energy by taking a tetrazolate-based Mn-MOF, $Mn_3[(Mn_4Cl)_3(BTT)_8(MeOH)]_2$ (H_3BTT = 1,3,5-tris(tetrazol-5-yl) benzene, MeOH = methanol) as the parent MOF.[39] The compound includes coordinatively unsaturated extra- and intra-framework Mn^{2+} ions with the anionic skeleton (Fig. 1). Despite soaking in concentrated methanolic solutions of MCl_2 (M = Fe^{2+}, Co^{2+}, Ni^{2+}, Cu^{2+}, Zn^{2+}) at room temperature for a month, all the MOF crystals maintained its integrity yet exchanged a significant amount of the framework cations, which was proved by powder X-ray diffraction (PXRD) and inductively coupled plasma-atomic absorption (ICP-AA). Notably, the Fe^{2+}, Co^{2+}, and Ni^{2+} experiments showed the substitution of only extra-framework cations, while the Cu^{2+} and Zn^{2+} cases indicated that the intra-framework cation substitution occurred at the $[Mn_4Cl]^{7+}$ cluster as well. With monovalent cations, meanwhile, either very little (Li^+) or negligible (Cu^+) amounts of cation exchange was observed at the extra-framework sites. Likewise, mixed-metal derivatives could be readily prepared by using this strategy, which might be impossible to access *via* direct syntheses. From this initial work, several informative interpretations are obtainable, revealing certain cation exchange behaviours. The fact that the MOF crystal maintained its integrity during the exchange process excludes the scenario of ligand transfer to a new cation and the creation of new MOFs. One can notice that different metal sites have different preferences for cation exchange, while the inserted cations also showed different exchange behaviours even for the same substituting sites. This can be explained by their different electronegativities of the metals.[53,54]

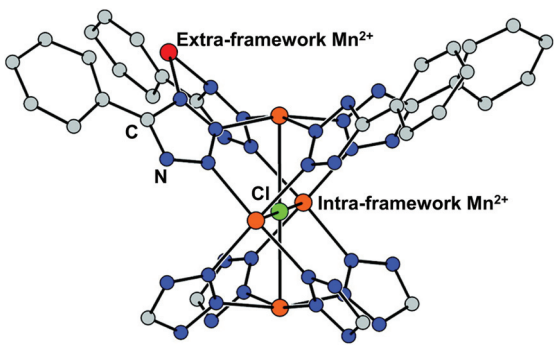

Fig. 1 Coordinatively unsaturated extra- and intra-framework (red and orange, respectively) Mn^{2+} ions in the crystal structure of Mn and tetrazolate-based metal–organic framework, $Mn_3[(Mn_4Cl)_3(BTT)_8(MeOH)]_2$. Reproduced with permission from ref. 40. Copyright 2007, American Chemical Society.

Many reports on the cation exchange process in MOFs have been published in the decade that followed the publication of this paper. Dincă *et al.*[36] surveyed those reports in 2014 and postulated four basic principles of cation exchange behaviours: (1) cation exchange of SBUs often occurred *via* open coordination sites, coordinating solvent molecules, or sites that could feature higher coordination numbers; (2) the weak field ligand environment of the SBUs enabled the coordinatively saturated metal sites to undergo cation exchange; (3) periodic trends existed depending on the types of cations (*e.g.*, Cu^{2+} exhibited stronger replacement tendency than other second row transition metals); and (4) the distortion allowance in the structure could determine the potential extent of cation exchange. As emphasised in follow-up studies, these principles have helped us determine whether the compounds and experimental conditions for cation exchange would be 'inert' or 'labile'.

The cation exchange method *via* simple soaking has been further modified to allow for its application for inert SBUs in MOFs. For example, UiO-66(Zr), a highly robust MOF that contains the $Zr_6O_4(OH)_4(CO_2)_{12}$ SBU, yielded Hf^{4+}-exchanged UiO-66(Zr/Hf) *via* soaking it in Hf^{4+} solution in dimethylformamide (DMF) while heating the mixture for 5 days at 85 °C.[55] In addition, the unprecedented bimetallic UiO-66(Zr/Ti) MOF was generated by soaking UiO-66(Zr) in a Ti^{4+} solution in DMF under the same experimental conditions described above (Fig. 2a). The Ti^{4+} analogue of the robust UIO-66(Zr) MOF could not be directly synthesised because Ti^{4+} is not known to form the $M_6O_4(OH)_4(CO_2)_{12}$ SBU structure of UIO-66 (Zr). Similarly, Dincă *et al.*[56] synthesised the unprecedented M-MOF-5 (M = Ti^{3+}, V^{2+}, V^{3+}, Cr^{2+}, Cr^{3+} Mn^{2+}, and Fe^{2+}), which also could not be obtained *via* direct synthesis (Fig. 2b). The authors indicated that the MOF-5 cluster acted as tripodal chelating ligand to construct the pseudo-tetrahedral geometry of MZn_3O (M = V^{2+}, Cr^{2+}, Mn^{2+}, and Fe^{2+}) and the pseudo-trigonal bipyramidal geometry of $ClMZn_3O$ (M = Ti^{3+}, V^{3+}, and Cr^{3+})

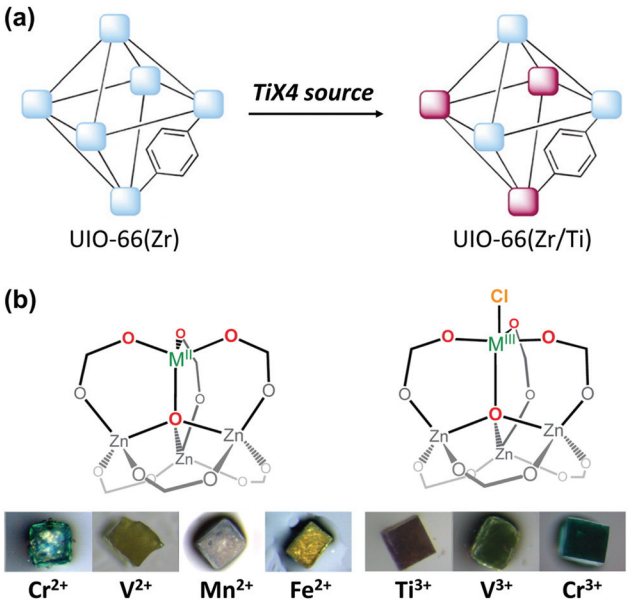

Fig. 2 Illustrations of post-synthetic cation exchange of (a) UiO-66 and TiX_4 (X = $TiCp_2Cl_2$, $TiCl_4$, or $TiBr_4$) and (b) MOF-5 after reacting with solutions of diverse metal salts. Reproduced with permission from ref. 55 and 56. Copyright 2012 and 2013, respectively, American Chemical Society.

which featured a terminal Cl^- moiety. These conventional solvothermal cation exchange methods typically require days or weeks and involve high energy consumption. To overcome these drawbacks, Zhou Long *et al.*[57] reported a microwave-assisted approach for substituting the Zr^{4+} ions with Ti^{4+} ions in UiO-66. Within a few hours, approximately half the Zr^{4+} ions in the SBUs were exchanged, the crystallinity of the MOF was well maintained, and its photocatalytic activity significantly improved.

2.2 Change of cation valence in SBUs

In addition to the cation exchange approach, SBU metal centres can undergo redox reaction, which is a critical issue to enhance functionality in MOFs. However, altering the oxidation states of the metal centres, the frameworks are very susceptible of structural collapse because of a drastic electron reorganization on charge *via* post-redox reactions. Nevertheless, this method is advantageous to producing mixed-valence MOFs or isostructural analogues with different cation valances, inaccessible by direct syntheses. In addition, many works showed that the redox of SBUs endows unexpected properties to the MOFs (Table 1). In 2004, Suh group synthesised a MOF of pillared-bilayer framework by assembling bismacrocyclic Ni^{2+} complex $[Ni_2(C_{26}H_{52}N_{10})(Cl)_4]$ and 1,3,5-benzenetricarboxylate (BTC).[40] The authors also performed an oxidation reaction in a DMSO/H_2O (1 : 1 v/v) solution of I_2 (0.0136 M) for 10 h, reducing the I_2 molecules to I_3^- anions in the channels, while two-thirds of the Ni^{2+} ions are oxidized to the low spin Ni^{3+} located in the framework. This yielded $[Ni_2(C_{26}H_{52}N_{10})]_3[BTC]_4(I_3)_4{\cdot}nI_2{\cdot}17H_2O$ *via* single-crystal-to-single-crystal transformation, which was amenable to X-ray diffraction structural analysis. Notably, this compound cannot be obtained directly by using a macrocyclic Ni^{3+} complex, which are stabilized in an octahedral geometry and thus have no coordination sites for ligands, and the Ni^{3+} species are easily reduced to Ni^{2+} in an aqueous media.

In contrast, Jeong *et al.*[42] reported the coordinative reduction of the paddlewheel Cu^{2+} SBUs in HKUST-1. Hydroquinone (H_2Q) was used as the reducing agent because it is an organic Lewis base that features lone-paired electrons. The reduction reaction was performed at 80 °C in acetonitrile (MeCN) solution of H_2Q under anhydrous conditions. During the reaction, the coordinating H_2Q molecule promptly dissociated into the $HQ^{\bullet}$ radical by transferring a single electron and donating a proton (Fig. 3a). Approximately 30% Cu^{2+} ions were reduced to Cu^+ ions, without being further reduced to Cu^0. This was attributed to the single-electron transfer, as revealed by single-crystal X-ray diffraction, ^1H nuclear magnetic resonance spectroscopy, and CO adsorption analyses. As illustrated in Fig. 3b, half of the reduced Cu^+ ions still remained in the SBUs, and presented pseudo-square planar geometry, while the other half protruded and transformed into $[Cu(MeCN)_4]^+$ complexes that were trapped in the small cages

Table 1 Metal–organic frameworks (MOFs) where secondary building units underwent redox reaction while maintaining MOF characteristics

Formula	Common name	Oxidation state variation	Extent	Agent	Conditions	Ref.
$[Ni_2(C_{26}H_{52}N_{10})_3[BTC]_4{\cdot}6$pyridine$\cdot36H_2O$	BOF-1	Ni^{2+} to Ni^{3+}	*ca.* 66%	I_2	DMSO/H_2O, 10 h	40
Fe_3TMQPTC	PCN-426-Fe	Fe^{2+} to Fe^{3+}	*ca.* 97%	Bubbled O_2	DMF, 15 min	41
Cr_3TMQPTC	PCN-426-Cr	Cr^{2+} to Cr^{3+}	*ca.* 91%			
$Cu_3(BTC)_2$	HKUST-1	Cu^{2+} to Cu^+	*ca.* 66%	H_2Q	MeCN, H_2Q,	42
Mn_2Cl_2(bbta)	MAF-X25	Mn^{2+} to Mn^{3+}	*ca.* 50%	H_2O_2	H_2O_2 in H_2O, MeCN, TEA, 2 days	43
$Ni(C_{10}H_{26}N_6)_3(bpdc)_3$	—	Ni^{2+} to Ni^{3+}	Unknown	Ag(I)	$AgNO_3$ in MeOH, 10 min + 18 h	44
$Cu_3(BTC)_2$	HKUST-1	Cu^{2+} to Cu^+	*ca.* 40%	MeOH	MeOH vapor, 200 °C, 10 h	45
$[\{Cu_{12}^{I}(trz)_8\}{\cdot}4Cl{\cdot}8H_2O]_n$	—	Cu^+ to Cu^{2+}	Unknown	Air	Air, several weeks	46
$[Cu(adp)(BIB)(H_2O)]_n$	—	Cu^{2+} to Cu^{3+}	Unknown	NaOH	H_2O_2 in NaOH,	47
$V^{III}(OH)(BDC)$	MIL-47(V^{III})	V^{3+} to V^{4+}	Complete	O_2	O_2, 150 °C, 2 h, 200 °C 1 h	48
$V_2^{III}(OH)_2C_{16}H_6O_8$	MFM-300(V^{III})	V^{3+} to V^{4+}	Complete	O_2	O_2, 150 °C, 16 h	49
Ce(BTC)	Ce(III)-MOF	Ce^{3+} to Ce^{4+}	*ca.* 25%	NaOH, H_2O_2	NaOH/H_2O_2, 2 min	50
Fe_2(dobdc)	Fe-MOF-74	Fe^{2+} to Fe^{3+}	Unknown	O_2	O_2	51
Fe(OH)(BDC)	MIL-100(Fe)	Fe^{3+} to Fe^{2+}	*ca.* 23%	Calcination	250 °C, 12 h	52

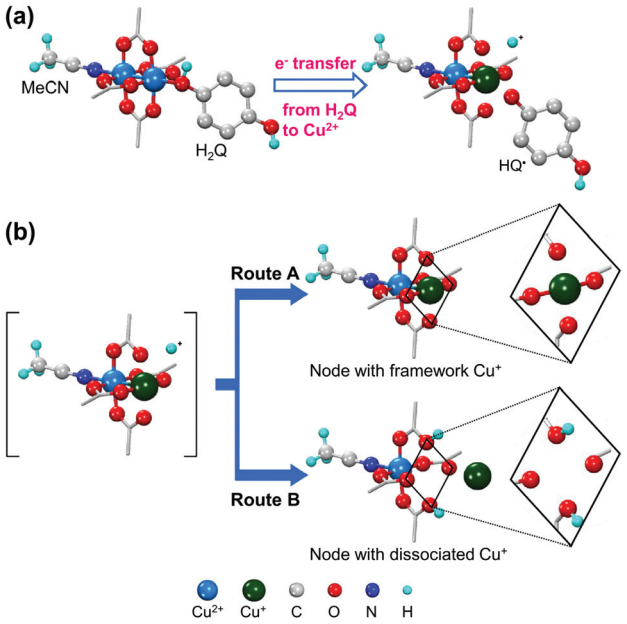

Fig. 3 Illustrations of (a) coordinative reduction of Cu^{2+} in paddlewheel node of HKUST-1 and (b) two possible routes for association of Cu^{+} ions with paddlewheel node or dissociation of Cu^{+} ions from framework. Here, H_2Q is hydroquinone. Reproduced with permission from ref. 42. Copyright 2019, American Chemical Society.

of HKUST-1. Likewise, using the proper reductant is the key to achieving mild and gradual changes in cation valence while retaining the integrity of the MOF structure. Notably, the use of common reductants, such as hydrides, only resulted in the structural degradation of HKUST-1 and formation of metallic Cu^0 nanoparticles, despite using exact stoichiometric amounts of reactants.

To obtain MOFs that feature oxidation states that could not be achieved using conventional synthesis methods, cation exchange using metal species that could readily change their oxidation states could be conducted first. This strategy was reported in 2014 by Zhou *et al.*[41] who synthesised PCN-426-Mg, that comprised $[Mg_3(\mu_3\text{-}O)]$ clusters of three Mg^{2+} octahedrons. Because the Mg–O bonds are relatively labile according to the HSAB theory, the synthesised MOF easily underwent cation exchange with common transition metal ions, and acted as template for the next step: changing the oxidation states. During this step, divalent cations (Fe^{2+} and Cr^{2+}) were first inserted to exchange the cations and preserve the structure of the MOF, then, they were oxidised to higher oxidation states (Fe^{3+} and Cr^{3+}) using a stream of air for 15 min while suspended in DMF. Conversely, when high-valence metals were used for direct synthesis, the MOFs scarcely crystallise because of the inertness of the pre-formed strong metal–ligand bonds during the synthesis reaction.[18,58–62]

2.3 Generation of defects of SBUs

Crystal defects indicate the presence of characteristic imperfections (or irregularities) of the host lattice, such as vacancies, compositional impurities, disorders, and dislocations.[37,38] For real-life systems, the crystalline materials mostly contain inherent defect sites, and therefore, so do MOFs. The defects decrease the crystallinity of MOFs and are considered to be detrimental for some applications, such as optoelectronics.[63] However, defects could also be advantageous for generating novel functions, such as higher porosity, higher sorption, and enhanced catalytic performance, which cannot be achieved using the original structures.

In broad terms, defective MOFs are frameworks that feature heterogeneous composition; in this sense, the afore-mentioned processes of cation exchange and oxidation state change can also be understood within defect chemistry and engineering if they occur incomplete and disordered. Nevertheless, among MOF scholars, the definition is typically considered to be the absence of linkers and/or metal nodes (*i.e.*, Schottky-type point defects). Thus, for differentiation, we will denote those types of defects as 'vacancy defects'. Moreover, this report strictly refers to the PSM methods that generate defects (mostly vacancies) in SBUs while preserving the characteristics of MOFs, as illustrated in the Venn diagram in Fig. 4. The report Li *et al.*[64] published in 2014 could help clarify the boundaries of definition. They used $Zn_4O(PyC)_3$ (PyC = 4-pyrazolecarboxylate) and eliminated the metals and linkers in the framework (Fig. 5). Upon the immersion of the MOF crystals in water, their structure underwent SCSC transformation, and their architectural stability was fully retained. This facilitated the crystallographic characterisation of the missing sites, *i.e.*, vacancies, *via* the removal of 25% of the metal ions and 50% of the linkers (structure **2** in Fig. 5). This metal and linker elimination reaction even varied the type of SBUs from octahedral to triangular ones. However, the resultant compounds would not be considered to be defective MOFs owing to the crystallographic transformation with ordered vacancies. Subsequently, those vacant sites were filled with other metal ions by immersing the MOF crystals in solutions of different metal ions, and the frameworks of heterometallic octahedral SBUs could be obtained.

According to Fischer *et al.*,[38] two methods are available for creating defect sites: a *de novo* synthesis (*e.g.*, modulation,

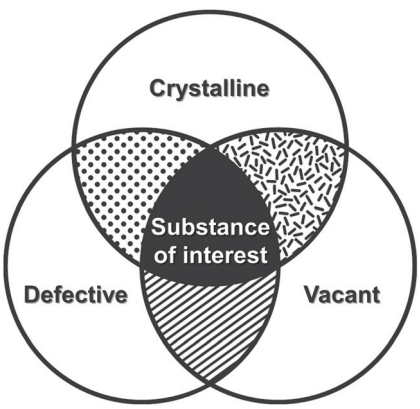

Fig. 4 Venn diagram of three properties of metal–organic frameworks after post-synthetic modification of secondary building units.

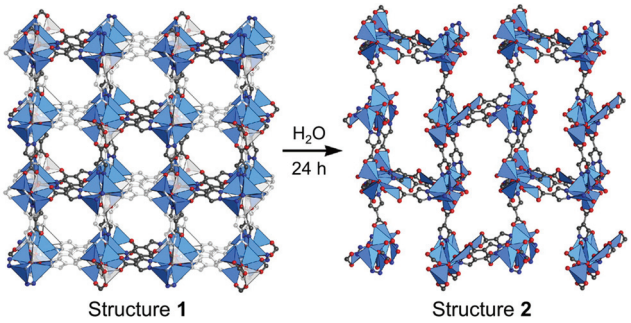

Fig. 5 Single-crystal structures of $Zn_4O(PyC)_3$ before and after the creation of ordered vacancies. Here, PyC is 4-pyrazolecarboxylate. Reproduced with permission from ref. 65. Copyright 2014, American Chemical Society.

mixed-linker approach, and fast crystal growth) and the PSM of pre-synthesised MOF crystals, including mechanical treatment, harsh activation, and acid/base treatment. For the PSM procedures, it is important that the MOF structure be tolerant of certain levels of missing constituents to prevent complete structure degradation. Therefore, the key for generating vacancy defects in SBUs would lie in finding highly defect-tolerant MOFs and/or partially decomposing the structure. In 2014, Guo *et al.*[65] reported the use of thermal decarboxylation to generate vacancy defects. They broke the Zn-carboxylate bonds of MOF-5, which were the weakest points of the structure that would be lost first upon heating. Structural characterisation revealed that MOF-5 annealed at 380 °C possessed local vacancy defects owing to the partial decomposition of carboxylates while maintaining the overall framework. In 2017, De Vos *et al.*[66] further developed this method using the mixed-linker UiO-66 that featured *trans*-1,4-cyclohexane-dicarboxylate (CDC) and 1,4-benzenedicarboxylate (BDC) as ligands. The relatively thermo-labile CDC linker was decomposed at 325 °C, whereas the BDC linker remained unchanged at this temperature. Advantageously, this process eliminated the CDC linker moieties completely and remained no by-products, unlike MOF-5, where benzoate moieties were detected in the framework after annealing.

In 2014, Lillerud *et al.*[67] observed that the concentration of missing linker defects of UiO-66 increased as the number of washings increased, which was attributed to its hydrolysis. Similarly, external solvents or chemicals often cause the cleavage of the framework bonds and the generation of defects. Therefore, the metal–carboxylate bonds of MOFs could be broken *via* deprotonation in acidic environment. For example, De Vos *et al.*[68] reported the use of acid treatment for the $Fe_3(\mu_3\text{-OH})$ SBU of MIL-100(Fe). As presented in Fig. 6a, soaking the MOF in common acids, including CF_3COOH and $HClO_4$, which are stronger acids than the BTC linker of MIL-100(Fe), generated defective Brønsted acid sites. Conversely, Kim *et al.*[69] recently proposed a Ag-catalysed decarboxylation, which involved HKUST-1 crystals, $AgNO_3$, and $K_2S_2O_8$. During the reaction, Ag^+ transferred two electrons to $S_2O_8^{2-}$ and was oxidised to Ag^{3+} while generating $SO_4^{\bullet-}$. The

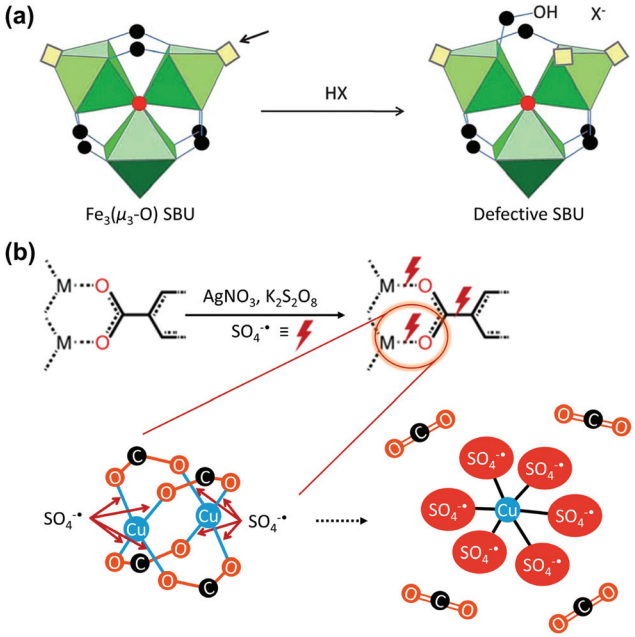

Fig. 6 Proposed vacancy-generation routes of (a) acid activation of the $Fe_3(\mu_3\text{-O})$ secondary building unit (SBU) using a protonic acid and (b) chemical etching *via* Ag-catalysed decarboxylation under mild conditions. Reproduced with permission from ref. 68 and 69. Copyright 2012, Royal Society of Chemistry, and Copyright 2018, Springer Nature, respectively.

generated $SO_4^{\bullet-}$ radical reacted with the square planar Cu^{2+} centre, and formed six-coordinated octahedral Cu-sulphate complexes; this was accompanied by decarboxylation, which generated CO_2. This Ag-catalysed decarboxylation reaction removed a C–C bond and directly cleaved the M–O bond, unlike the conventional decarboxylation methods.

2.4 Incorporation of new species into SBUs

Open metal sites (OMSs) are a noteworthy feature of MOFs, and could be used as catalytic or specific adsorption sites. In addition, OMSs can be functionalised *via* coordination bonds between them and functional organic molecules (Table 2). For example, Long *et al.*[70] synthesised and functionalized Mg_2(dobpdc) (H_4dobpdc = 4,4′-dihydroxy-(1,1′-biphenyl)-3,3′-dicarboxylic acid) by coordinating a diamine ligand at its five-coordinated OMS (Fig. 7a). Aqueous amine solutions are widely utilised as CO_2 absorbents for amine scrubbing systems owing to their high affinity for CO_2. Therefore, combining the amine functional group with Mg_2(dobpdc) achieved a synergistic effect for capturing CO_2. Recently, Chen *et al.*[71] decorated the $Fe_3(\mu_3\text{-OH})$ SBUs of flexible MIL-88B with coordinating molecules: 4-cyanopyridine, 4-ethynylpyridine and 4-vinylpyridine, which contained unsaturated nitrile, ethynyl, and vinyl groups, respectively, for [2 + 2 + 2] cyclotrimerisation. Owing to the confined porous environment with suitable orientation, the incorporated monomers could undergo cyclotrimerisation and generated trimeric products. This consecutive incorporation of

Table 2 Metal–organic frameworks (MOFs) where secondary building units underwent coordinative incorporation of organic species

MOF	Incorporated molecule	Incorporated position in SBU	Applications	Ref.
Mg_2(dobpdc)	Dimethylethylenediamine	OMS	Capture	70 and 78
Mg_2(dobpdc)	2,2-Dimethyl-1,3-diaminopropane	OMS	Capture	100
Mg_2(dobpdc)	2-(Aminomethyl)piperidine	OMS	Capture	79
Ni-MOF-74	Imidazole	OMS	Separation Magnetic	87 and 101
HKUST-1	4-(Methylamino)-pyridine	OMS	Capture	102
HKUST-1	Tetracyanoquinodimethane	OMS	Conductivity	94
HKUST-1	H_2O	OMS	Proton conductor	96
MIL-101(Cr)	L-Proline	OMS	Catalysis	103
MIL-101(Cr)	Ethylenediamine	OMS	Catalysis	104
UIO-66	Li^{t}BuO	μ_3-OH	Detoxification	90
UIO-66	SO_4	Terminal –OH/H_2O	Catalysis	105
NH_2-UIO-66	Phenylsilane	Termianl –OH	Hydrophobicity	106
NU-1000	Perfluoroalkane	Terminal –OH/H_2O	Capture	72
NU-1000	Boron-dipyrromethene	Terminal –OH/H_2O	Detoxification	107
NU-1000	Non-polar organic carboxylate	Terminal –OH/H_2O	Water stability	108
MOF-808	SO_4	Terminal –OH/H_2O	Catalysis	109 and 110
MOF-808	Trimethylsilyl triflate	Terminal –OH/H_2O	Catalysis	111
MOF-808	Ethylenediaminetetraacetic acid	Terminal –OH/H_2O	Capture Proton conductor	97 and 99

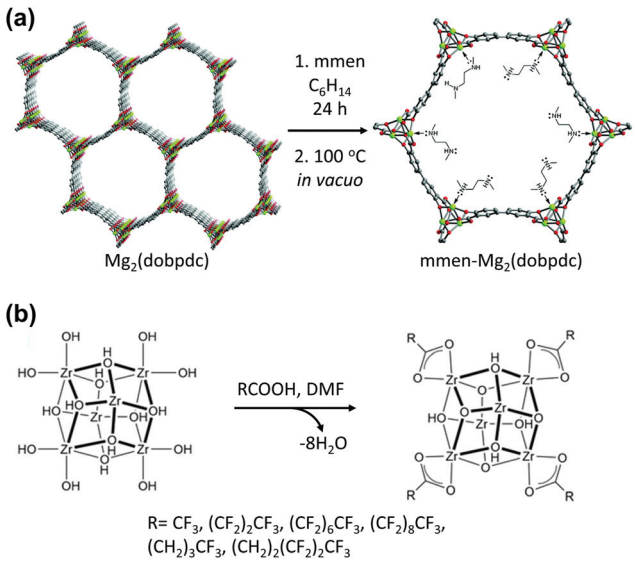

Fig. 7 (a) Synthetic route for the alkylamine-appended mmen-Mg_2(dobpdc) (mmen = *N*,*N*′-dimethylethylenediamine and H_4dobpdc = 4,4′-dihydroxy-(1,1′-biphenyl)-3,3′-dicarboxylic acid) and (b) solvent assisted ligand incorporation approach for functionalisation of perfluoroakane. Here, DMF is dimethylformamide. Reproduced with permission from ref. 70 and 72. Copyright 2012 and 2013, respectively, American Chemical Society.

monomers followed by PSM *via* chemical reaction transformed the flexible MIL-88B into a rigid framework of unprecedentedly large void volume. Farha *et al.*[72] decorated the Zr_6 SBUs of NU-1000 with perfluoroalkane to form defect-free NU-1000 that comprised $[Zr_6(\mu_3\text{-}OH)_8(\text{–}OH)_8]^{8+}$ clusters with carboxylate linkers (Fig. 7b). Similar to the OMS-containing MOFs, these Zr_6 SBUs allowed the addition of functional species to it. The functional ligand could be coordinated to the Zr_6 SBUs by replacing the terminal OH–/H_2O groups *via* the acid–base reaction known as solvent-assisted ligand incorporation. Thus, the generated perfluoroalkane-functionalised NU-1000 exhibited high CO_2 affinity owing to the presence of the C–F dipoles of the introduced ligand which interacted with the CO_2 quadrupole.

Using a similar ligand installation procedure on a Zr-based MOF, Zhou *et al.*[73] synthesised a mixed-linker Zr-MOF which could not be obtained *via* one-pot synthesis owing to the thermodynamic unfavorability of the process (Fig. 8). PCN-700, a Zr-based MOF, consists of eight-connected $Zr_6O_4(OH)_8(H_2O)_4$ with two vacant pockets (A and B, 16.4 and 7.0 Å in length, respectively) between neighbouring SBUs. By inserting linkers of the suitable size into the pockets, mixed-linker structures were successfully obtained *via* a kinetically controlled synthetic pathway. Because the BDC linker (6.9 Å) was fitted to pocket B, the PCN-701 structure was constructed *via* sequential installation by replacing the terminal OH–/H_2O groups of the Zr SBU, accompanied by the slight elongation of pocket A to 16.5 Å (pocket A′). Because the biphenyl rings of BPDC (BPDC = biphenyl-4,4′-dicarboxylate) allow for changes in the dihedral angle from 78.1° to 89.5°, the framework could self-adjust its structure. Similarly, pocket A was linked with a Me_2-TPDC (TPDC = *p*-terphenyl-4,4″-dicarboxylate) linker to construct PCN-702 and pocket B was lengthened to 8.2 Å (pocket B′). Because only the slight elongation of pocket A was induced *via* the installation of the BDC linker, Me_2-TPDC was installed into pocket A′ to construct PCN-703, which generated the elongated pocket A″ (17.4 Å). However, pocket B′ was too large to bridge the BDC linker, and therefore PCN-703 could not be constructed using PCN-702. As such, multiple functional groups could be installed to the coordinatively unsaturated Zr_6 clusters in a crystallographically controlled manner. Following

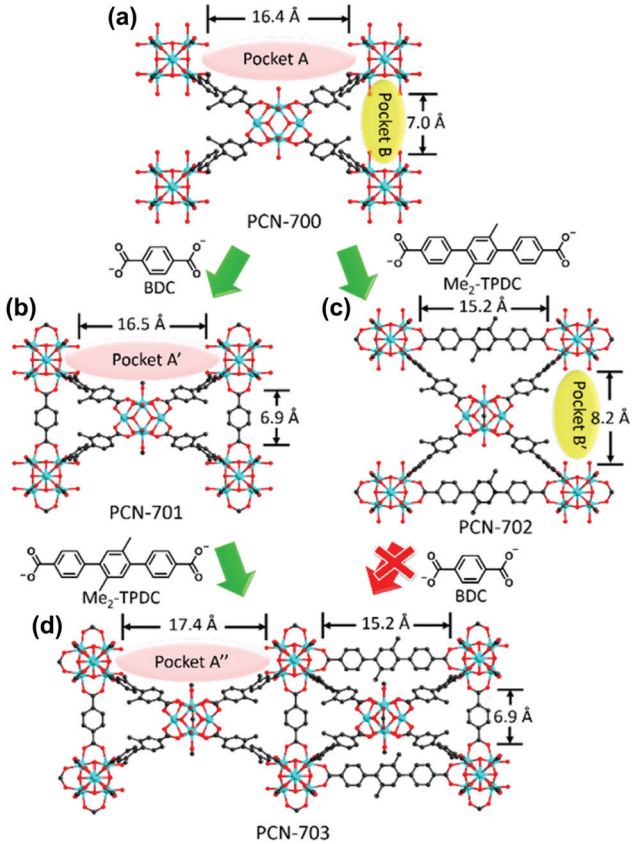

Fig. 8 Structures of (a) PCN-700, (b) PCN-701, (c) PCN-702 and (d) PCN-703. Here, BDC and TPDC are 1,4-benzenedicarboxylate and *p*-terphenyl-4,4″-dicarboxylate, respectively. Reproduced with permission from ref. 73. Copyright 2015, American Chemical Society.

this study, Zhou *et al.*[74] more extensively controlled the arrangement of functionalities in PCN-700 using linkers of different lengths and/or substituents.

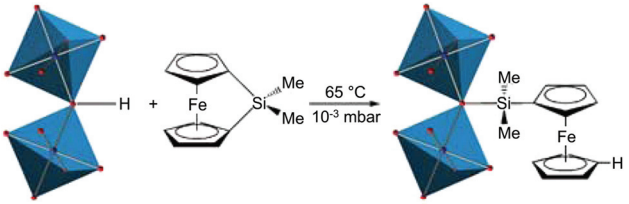

Fig. 9 Ring-opening reaction of the bridging HO-group in the secondary building units of MIL-53(Al) and 1,1′-ferrocenediyl-dimethylsilane. Reproduced with permission from ref. 75. Copyright 2009, American Chemical Society.

In addition to decoration with organic ligands, incorporation of inorganic complexes to impart functionalities that cannot be observed in organic species has being extensively studied (Table 3). Fischer *et al.*[75] first combined the inorganic complex, 1,1′-ferrocenediyl-dimethylsilane with MIL-53(Al) that consisted of an Al^{3+} cation node and bridging OH group (Fig. 9). Because the bridging OH group was available for functionalisation, the Si atoms of the ferrocene complex could bind to the OH site followed by the migration of protons to the η^5-C_5H_5 rings, which resulted in the slight improvement in the catalytic performance of the MOF. Gates *et al.*[76] introduced Ir complexes ($Ir(CO)_2$ and $Ir(C_2H_4)_2$) to UiO-66 and NU-1000 by reacting Ir precursors, $Ir(CO)_2(acac)$ ($acac^-$ = acetylacetonate) and $Ir(C_2H_4)_2(acac)$, with the OH–/H_2O sites. The Zr_6 clusters of UIO-66 and NU-1000 could be decorated with inorganic complexes owing to their defective OMSs in the SBUs, which were occupied by OH–/H_2O functional groups. Zaworotko *et al.*[77] reported a PSM approach that represents the transformation from dinuclear Cd^{2+} SBUs to novel tetranuclear Cu^{2+} SBUs, *via* stepwise metal ion exchange and metal salt incorporation. During the transformation, the Cu^{2+} paddlewheels derived from Cd^{2+} ones bound two more Cu^{2+} cations to form a Cu_4 intermediate, and subsequently underwent the mole-

Table 3 Metal–organic frameworks (MOFs) where secondary building units underwent coordinative incorporation of metal species

MOF	Incorporated metal	Incorporated position in SBU	Applications	Ref.
NU-1000	Zn, Al	Terminal –OH	Catalysis	112
NU-1000	Ir(III)	Terminal –OH/H_2O	Catalysis	113
NU-1000	Cu(II)	Terminal –OH	Catalysis	89
NU-1000	In-Me_3	Terminal –OH/H_2O, μ_3-OH	Catalysis	114
NU-1200	Vanadium oxide	Terminal –OH/H_2O	Catalysis	115
UIO-66	Cu	Terminal –OH/H_2O	Catalysis	88
NH_2-UIO-66	Ti(IV)	Terminal –OH/H2O	Catalysis	116
UIO-68(Zr)	Co–Cl	μ_3-OH	Catalysis	117
Zr_{12}-bpdc MOF	Cu(I)	μ_2-OH, μ_3-OH	Catalysis	118
Zr-MTBC	Co	μ_2-OH, μ_3-OH	Catalysis	119
Ti_8-BDC MOF	Co	(μ_2-O), (μ_2-O^-)	Catalysis	120
TPHN-MOF	Mg–Me	μ_3-OH	Catalysis	121
Zr_{12}-TPDC	Co–H	μ_2-OH, μ_3-OH	Catalysis	122
PCN-700	Ni	Terminal –OH/H_2O, μ_3-OH	Catalysis	123
MOF-808	Pd	Terminal –OH/H_2O	Catalysis	124
Hf-MOF-808	Vanadium oxide	Terminal –OH/H_2O	Catalysis	125
MIL-53(Al)	Ferrocene	–OH group	Electrochemical system	75
MIL-125	NiH	μ_2-OH	Catalysis	126

cular rearrangement to generate the tetrametallic $[Cu_4X_2(COO)_6(H_2O)_2]$ SBU (X = CH_3O^-, OH^-).

3. Property modulation and applications *via* SBU alteration

Four approaches for the alteration of SBUs were summarised and discussed in the previous section. Relevant studies over the last two decades have indicated that even minor alterations of SBUs could significantly influence the physicochemical properties of MOFs, and could engender novel functions. Therefore, in this section, several representative results are discussed where SBU alterations successfully modified the MOF properties, and rendered them useful for applications such as sorption, separation, and catalysis.

3.1 Sorption properties

To overcome the microporosity of MOFs and enhance the ability to capture larger molecules, hierarchically porous MOFs have been studied. Recently, Sun *et al.*[45] achieved hierarchical porosity in HKUST-1 by reducing Cu^{2+} to Cu^+ using CH_3OH vapor at 200 °C as a reducing agent. The resultant compound was used to capture thiophene, a large aromatic sulphide molecule, which was too large and could not be captured using pristine HKUST-1. Similar to the case of H_2Q-treated HKUST-1, Cu^{2+} changed its coordination geometry to two-coordinated complex by releasing two of the four carboxylates on the paddlewheel SBU. The interaction between the aromatic sulphide molecule and Cu^+ *via* robust phi-complexation rendered this hierarchically porous MOF a good thiophene adsorbent. The amounts of Cu^+ and resulting mesopores were controlled by tuning the reaction time. The optimum MOF for thiophene capture was obtained after 10 h, and comprised 30 nm mesopores and 44% Cu^+ ions.

As described above, Mg_2(dobpdc) decorated with *N*,*N*′-dimethylethylenediamine (mmen) presented large CO_2 capture capacity and high efficiency owing to the phase-changing properties that contributed to unusual step-shaped adsorption isotherm.[73,78] As illustrated in Fig. 10, mechanistically, the capturing process followed several steps: first, the coordinated amine was deprotonated by the neighbouring amine, which could act as strong base and led to the formation of ammonium groups. CO_2 was simultaneously added to the coordinated amine and formed a carbamate species. This ammonium carbamate species destabilised the coordinated neighbouring amine and facilitated the cooperative insertion of CO_2 molecules between the metal and amine groups *via* a chain reaction. Consequently, this mmen-decoration approach on Mg_2(dobpdc) led to the enhanced CO_2 capture performance of the MOF under flue gas conditions (15% CO_2 in N_2 at 40 °C), and the low energy consumption for the process. Very recently, 2-(aminomethyl)piperidine was incorporated into the same MOF, and a significant improvement of CO_2 uptake was achieved even under high humidity conditions, which has been considered to be a significant drawback for the practical use of this MOF in flue gas environment.[79]

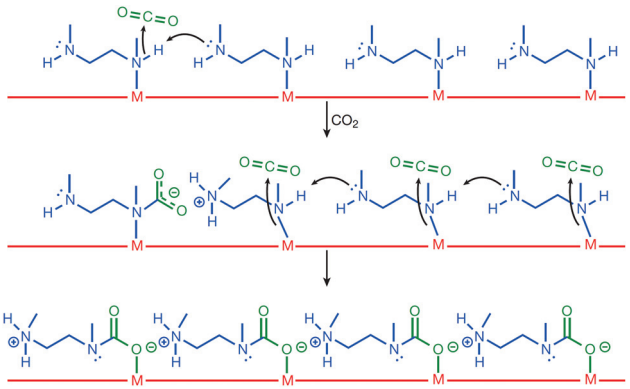

Fig. 10 Mechanism for CO_2 adsorption at four neighbouring M-mmen sites within an infinite one-dimensional chain of such sites running along the channel of a mmen-M_2(dobpdc) compound. Here, mmen is *N*,*N*′-dimethylethylenediamine. Reproduced with permission from ref. 78. Copyright 2015, Springer Nature.

3.2 Gas separation

Unlike conventional gas mixture separation that could be conducted *via* simple molecular sieving,[80] the isotope mixture separation procedure requires special techniques owing to the almost identical properties of the isotopes. Therefore, researchers have recently used nanoporous materials to separate hydrogen isotopes using two types of the so-called 'quantum sieving effect'. Heavier isotopes with shorter de Broglie wavelength possess higher mobility than lighter isotopes in confined spaces, where the size difference between the pores and molecules becomes comparable to the de Broglie wavelength, which results in the enrichment of the product with heavier isotope materials. This phenomenon is known as kinetic quantum sieving (KQS), and thus, it is important to design a porous material that contains optimal pore size (3.0–3.4 Å).[81,82] Another quantum sieving mechanism, chemical affinity quantum sieving (CAQS), has been proposed to separate hydrogen isotopes *via* the strong interaction sites with hydrogen molecules, such as OMSs, where the heavier molecular mass of deuterium (D_2) led to the higher adsorption enthalpy and resulted in its preferential adsorption.[83,84]

To achieve such quantum sieving effects in MOFs, SBU alteration methods can be utilised. Heine *et al.*[85] used Cu(I)-MFU-4l, which exhibited high adsorption enthalpies for hydrogen molecules (32 kJ mol^{-1}) for this purpose. Cu(I)-MFU-4l was synthesised by replacing half of the terminal Zn sites with Cu^{2+} followed by exchanging the Cl^- ions with formate and subsequent heating under vacuum for 1 h.[86] At high temperature (above 90 K), the difference in the adsorption enthalpies of D_2 and H_2 was large (2.5 kJ mol^{-1}), which was attributed to the strongly binding Cu(I) sites that exhibited the high selectivity of 11. Recently, we described the imidazole-decorated Ni-MOF-74 (left side of Fig. 11).[87] Ni-MOF-74 is known to be one of the most effective H_2/D_2 separation materials owing to its

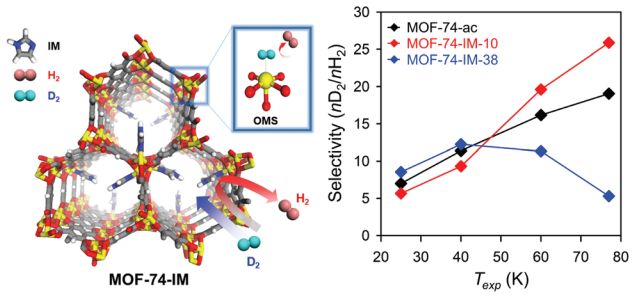

Fig. 11 Selectivity of MOF-74-IMs as function of exposure temperature (T_{exp}) after exposure to 1 : 1 H_2/D_2 mixture. Here, OMS is open metal site. Reproduced with permission from ref. 87. Copyright 2017, American Chemical Society.

high isosteric heat of adsorption for hydrogen *via* OMSs, and also its optimal pore size achieved *via* SBU alteration. The partially occupied imidazole molecules in the OMSs of Ni-MOF-74 could act as diffusion barrier and enhance the KQS effect by modifying the pore structures; moreover, the remaining OMSs provided selectively strong binding sites which exhibited CAQS effect. Based on control experiments on the degree of occupancy, 10% of imidazole decoration on the OMSs of Ni-MOF-74 (MOF-74-IM-10, right side of Fig. 11) presented the highest D_2/H_2 selectivity (26 at 77 K).

3.3 Catalysis

The catalytic activity of MOFs is typically attributed to the metal centres of SBUs, which could act as Lewis acidic sites. The report published by Long *et al.*[57] in 2017 is an interesting example, and described inducing photocatalysis *via* the microwave-induced cation exchange of $Zr_6O_4(OH)_4$ SBU in UiO-66 with Ti^{4+} ions. The energy band of pristine UiO-66(Zr) was calculated to be 4.00 eV using UV–vis spectroscopy and Mott–Schottky measurements. This indicated that pristine UiO-66 (Zr) presented n-type semiconductor characteristics and its photocatalytic activity towards the reduction of Se^{6+} was almost negligible. Conversely, the cation exchange product of UiO-66(Zr/Ti) (50% cations exchanged) presented the energy band value of 3.75 eV because the inserted Ti^{4+} cations increased the lower level of the conduction band. As illustrated in Fig. 12, because the probability of the electron transfer from the excited BDC linker to Ti^{4+} was higher than that from the excited BDC linker to Zr^{4+}, Ti^{4+} and Zr^{4+} acted as electron acceptor and trap, respectively, and thus, Ti^{4+} in the $(Ti^{4+}/Zr^{4+})_6O_4(OH)_4$ SBU could donate electrons to Zr^{4+} more easily. This improved the photocatalytic performance for the reduction of Se^{6+} by increasing the interfacial charge transfer from the linker to the metal SBU.

Incorporating new metal species into SBUs is another facile method for imparting additional catalytic activities to MOFs. Behm *et al.*[88] recently synthesised a Cu/UiO-66 catalyst for CO oxidation, where single Cu metal was deposited into SBUs. After soaking the UiO-66 crystals in a Cu^{2+} solution in DMF at 85 °C, it was observed that Cu^{2+} was coordinatively bridged to

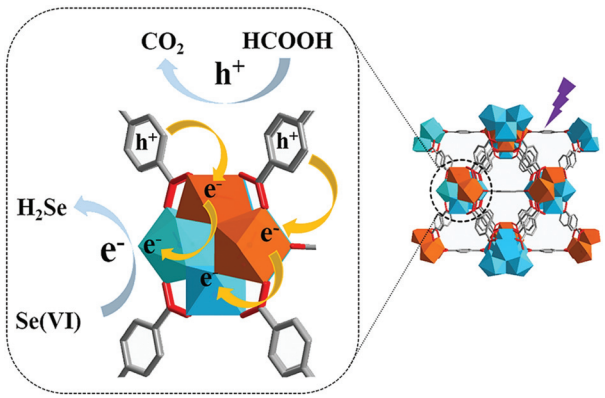

Fig. 12 Proposed mechanism for enhanced photocatalytic performance of UiO-66(Zr/Ti). Here, the Zr^{4+} and Ti^{4+} ions are blue and orange, respectively. Reproduced with permission from ref. 57. Copyright 2017, Royal Society of Chemistry.

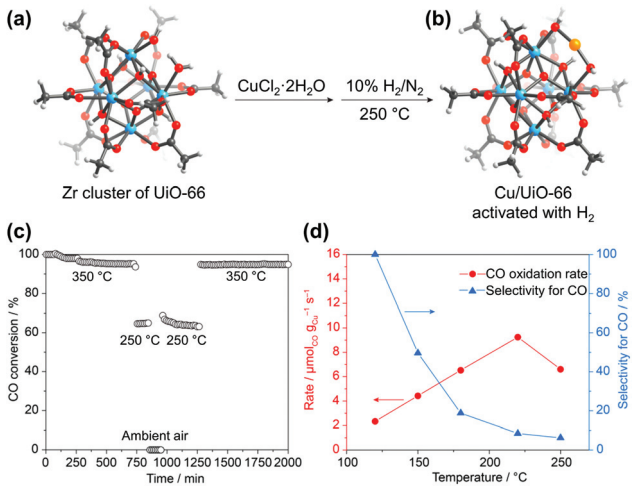

Fig. 13 Secondary building unit structures of (a) UiO-66 and (b) Cu/UiO-66. (c) CO conversion at different temperatures (cooling and shut-down of the reaction, and restart by heating in a reaction gas mixture), and (d) reaction rates of CO oxidation upon cycles. Here the Zr^{4+} and Cu^{+} ions are blue and orange, respectively. Reproduced with permission from ref. 88. Copyright 2019, American Chemical Society.

the OH–/H_2O terminal groups of the defective Zr_6 SBU in UiO-66 along with coordinated Cl^-. The attached Cu sites were again reduced to active Cu^+ species, and the Cl^- ions were removed *via* subsequent activation with H_2 (Fig. 13). The CO oxidation activity of this single-Cu catalyst was at least three times higher than that of conventional catalysts, such as Cu/CeO_2 and Cu/ZrO_2, even under O_2-rich atmosphere. Similarly, Lercher *et al.*[89] synthesised Cu-oxo dimer-supported NU-1000, by depositing Cu^{2+} ions on the Zr_6 SBU followed by oxidation at 200 °C in O_2 atmosphere. The resultant catalyst was able to oxidise methane to methanol with high efficiency under the methane pressure of 1 bar at 150 °C.

Detoxification of chemical warfare agents (CWAs) is one of the most important research fields where MOFs are used as

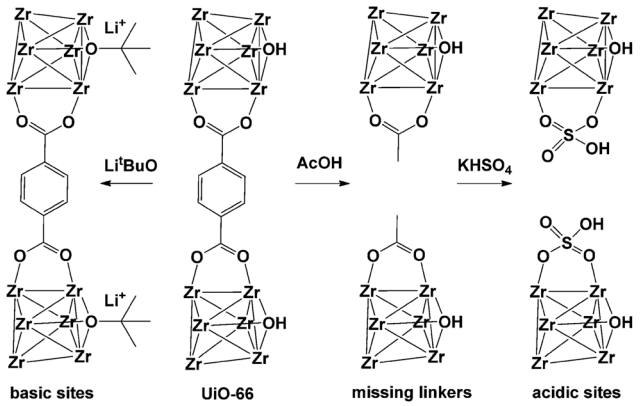

Fig. 14 Improvement of catalytic activity of $[Zr_6O_4(OH)_4(bdc)_6]$ (UiO-66) by introducing missing-linker defects and/or acidic and basic sites in its structure. Reproduced with permission from ref. 90. Copyright 2015, Wiley VCH.

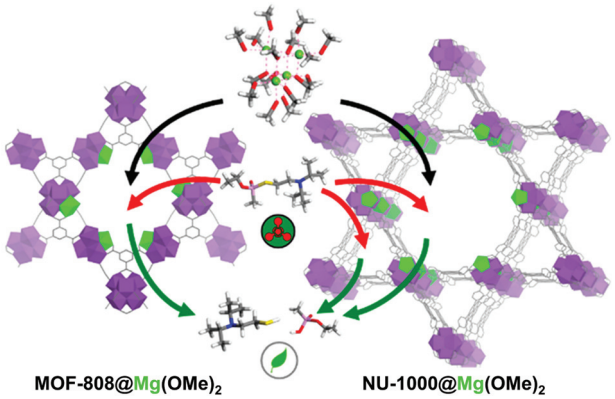

Fig. 15 Schematic representation of post-synthetic modification of metal–organic framework mesopores with $[Mg(OMe)_2(MeOH)_2]_4$ to yield $MgZr_5O_2(OH)_6$ clusters (Mg is highlighted in green) and ulterior detoxification of nerve agents that took place in the pore structure of MOF-808@$Mg(OMe)_2$ and NU-1000@$Mg(OMe)_2$. Reproduced with permission from ref. 91. Copyright 2019, American Chemical Society.

catalysts. UiO-66 presumably contains different types of inherent or intentionally created defects. In 2015, Navarro *et al.*[90] reported the reaction of activated pristine UiO-66 with Li^{t}BuO and introduced additional basic catalytic sites to UiO-66 by replacing the μ_3-OH sites in its SBUs (Fig. 14). In addition, UiO-66 was also reacted with acetic acid and $KHSO_4$, stepwise, which generated additional acidic sites (UiO-66@SO_4H) that could control the degradation activity of various CWAs. UiO-66@Li*O*t*Bu presented good performance for the degradation of CWA analogues, particularly diisopropylfluorophosphate (DIFP) (turnover frequency (TOF) = 0.13 min^{-1}), while both UiO-66@AcOH and UiO-66@SO_4H exhibited relatively low CWA degradation kinetics and conversion ratios.

Despite the significantly enhanced degradation ability caused by the incorporated lithium alkoxide moieties, the material was still air-sensitive and could not be utilised for real-life systems. Recently, Navarro *et al.*[91] investigated the substitution of the $Zr_6O_4(OH)_4$ SBUs of NU-1000, MOF-808, and UiO-66 with $MgZr_5O_4(OH)_4$, which involved a basic magnesium alkoxide and exhibited good catalytic activity and excellent sustainability. For this process, $[Mg(OMe)_2(MeOH)_2]_4$ was used as Mg precursor and replaced one Zr site for each SBU of NU-1000 and MOF-808 with $Mg(OMe)_2$ (Fig. 15). UiO-66 did not undergo cation exchange because its pores could not accommodate the bulky Mg complex. MOF-808@$Mg(OMe)_2$ exhibited significantly high degradation performance for DIFP (TOF = 0.26 min^{-1}) compared with pristine MOF-808 (TOF = 0.01 min^{-1}). In addition, this compound could retain its activity for 20 days, while the activity of UiO-66@Li*O*t*Bu was significantly decreased within a month. That was attributed to the incorporation of $Mg(OMe)_2$ in the centre of the SBUs, whereas Li^{t}BuO was located at the periphery of SBUs. NU-1000@$Mg(OMe)_2$ also exhibited good catalytic activity, but lower than that of MOF-808, because the nerve agents could access the Mg-decorated mesopores and non-decorated micropores of NU-1000, which led to the lower exposure of the agents to catalytic Mg^{2+} sites, as explained using the Monte Carlo simulation.

3.4 Electron conductivity

Low electron conductivity is one of the drawbacks of MOFs, and thus it is a hindrance for the use of MOFs for many practical applications. The intrinsic design and synthesis of conductive MOFs are very challenging because MOFs present low atomic density and are usually constructed *via* the coordination between hard metal ions and redox-inactive organic ligands. This brings about significant differences in orbital energy between bonding atoms and reduces orbital overlap, which leads to the charge carriers being energetically trapped on lattice sites. Consequently, typical MOFs present little or no band dispersion and behave as insulators. To construct electrically conductive MOFs by closing the electronic band gap, two basic strategies can be used: the use of redox-active components in *de novo* synthesis processes and doping or introducing defects that could increase the electron conductivity of the MOFs. Using the second strategy, one can move the Fermi level of the structures to increase the charge carrier concentration in the band gap. Nonetheless, the goal is to facilitate charge transport *via* the lattice sites of MOFs and to lower their band gap so they can conduct electricity.[92,93]

In 2014, Allendorf *et al.*[94] reported engendering and controlling the conductivity of HKUST-1 by introducing redox-active 7,7,8,8-tetracyanoquinodimethane (TCNQ) molecules to its OMSs. As depicted in Fig. 16, the TCNQ molecules bridged two Cu paddlewheel SBUs; moreover, *ab initio* calculations revealed that TCNQ could strongly bind to the MOF (binding energy of 83.9 kJ mol^{-1}) and insert unoccupied molecular orbitals into the band gap of the MOF, thus creating new charge transfer paths and enabling electronic coupling between the HKUST-1 framework and TCNQ. The importance of guest–host interactions was further demonstrated by replacing TCNQ with its fully hydrogenated form, (cyclohexane-1,4-diylidene)dimalononitrile (H4-TCNQ), which lacked a conjugated π electron network. Consequently, the electron conductivity of the obtained MOF was poor. Conversely, when 2,3,5,6-tetrafluoro-

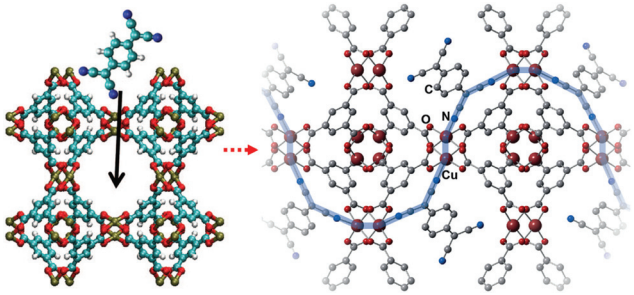

Fig. 16 Addition of 7,7,8,8-tetracyanoquinododimethane molecules to HKUST-1 and suggested electron pathway through the framework. Reproduced with permission from ref. 94 and 93. Copyright 2014, American Association for the Advancement of Science, and Copyright 2016, Wiley VCH.

7,7,8,8-tetracyanoquinodimethane (F4-TCNQ), which presented similar band gap with, but higher electron affinity then TCNQ, was introduced to the OMSs of HKUST-1, the obtained MOF presented lower conductivity than HKUST-1, because the high electron affinity of F4-TCNQ inhibited electron mobility. Volkmer *et al.*[92] used the cation exchange method and reported the modulation of the band gap and electron conductivity of MFU-4. Exchanging the octahedral Zn sites of the SBUs with Co^{2+} cations (*i.e.*, Co-MFU-4), the highest occupied molecular orbital energy state of Co-MFU-4 was no different than that of MFU-4 (−6.14 eV) as it originated from the ligand, while the insertion of the partially occupied d-orbitals of CO^{2+} generated bands below the lowest unoccupied molecular orbital energy state of the ligand, and subsequently decreased the band gap.

3.5 Proton conductivity

Many studies on proton conducting MOFs have mostly focused on the introduction of guest molecules/ions and the incorporation of functional groups. In particular, the guests accommodated in pores, such as water and imidazole, could act as proton source, and provide proton transfer pathways *via* hydrogen bonding.[95] The proton conductivity of MOFs could be significantly increased by incorporating guest molecules and also by decorating SBUs with proper functional molecules. Hupp *et al.*[96] investigated the relationship between the proton conductivity and coordination environment at the SBUs of HKUST-1. The OMSs of HKUST-1 were initially coordinated with synthetic solvent molecules, such as H_2O and ethanol (EtOH), and could be substituted with other coordinating solvent molecules, such as methanol (MeOH) and MeCN. As depicted in Fig. 17a. The MOF that contained H_2O-coordinated Cu^{2+} and MeOH molecules in the pores exhibited much larger proton conductivity (15 μS cm^{-1}) than the MOF that contained only pristine MeOH in the pores (0.17 μS cm^{-1}). In contrast, EtOH- or MeCN-coordinated Cu^{2+} moieties did not present any increase in proton conductivity (0.2 μS cm^{-1}). This result was attributed to MeOH molecules being protonated by coordinating H_2O molecules, and the increased concentration of protonated MeOH increased the proton conductivity of the MOF. Conversely, the MeCN-coordinated compound lacked dissociable protons for MeOH, and therefore, it could not improve the proton conductivity of the target. Because the acidity of EtOH is slightly lower than that of MeOH (pK_a of 15.9 and 15.5, respectively), the increase in conductivity of the EtOH-coordinated HKUST-1 should also be limited. Such functional groups modified the pore environment and generated an abundance of carboxyl groups by substituting the detachable formate anions grafted to the SBUs.[97] The resultant MOF-808-OX exhibited higher proton conductivity (1.94×10^{-4} S cm^{-1}) than pristine MOF-808 (1.25×10^{-6} S cm^{-1}).

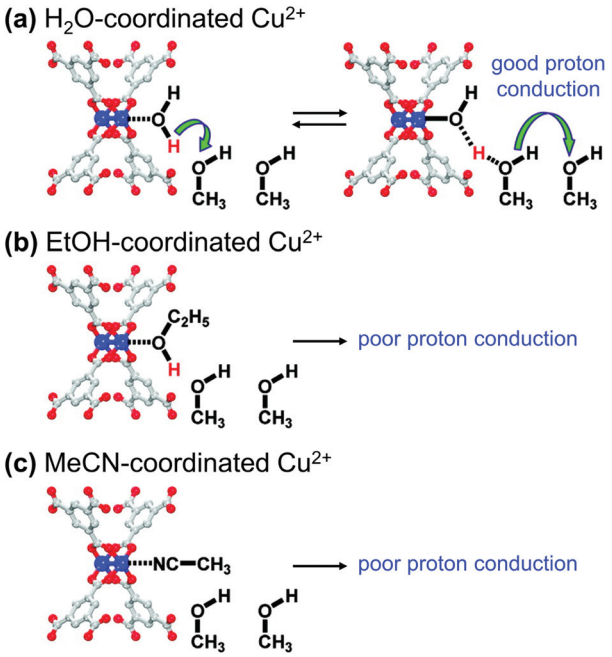

Fig. 17 Qualitative representations of proton transfer from Cu^{2+} sites coordinated with (a) H_2O, (b) ethanol (EtOH), and (c) acetonitrile (MeCN). Reproduced with permission from ref. 96. Copyright 2012, American Chemical Society.

3.6 Sensing

Chemical sensing of metal ions in MOFs usually occurs *via* coordinative ligand or is induced by guest molecules. If MOF cation exchange could occur in fast and easily detectable fashion, it can be exploited for the sensing of metal cations.[31] Yan *et al.*[98] utilised MIL-53(Al) to "turn-off" the detection of Fe^{3+}, as this MOF quenched the fluorescence emission that resulted from the ligand-to-metal charge transfer from the BDC moieties to the Al^{3+} cations. Of various aqueous cation solutions, including K^+, Na^+, Ca^{2+}, Mg^{2+}, Cu^{2+}, Zn^{2+}, Co^{2+}, Mn^{2+}, Ni^{2+}, Hg^{2+}, Cd^{2+}, Pb^{2+}, Fe^{2+}, Fe^{3+}, Cr^{3+}, and Al^{3+}, only Fe^{3+} presented quenching effect for MIL-53(Al) within the 3–200 μM concentration range, and thus, MIL-53(Al) could be utilised for selective Fe^{3+} sensing. In 2018, Zhong *et al.*[99] adopted ethylenediaminetetraacetic acid (EDTA) as decorating functional group with many coordination sites (four hard car-

boxyl groups and two softer tertiary amine groups) and MOF-808, which consisted of $Zr_6O_4(OH)_4$ SBUs and BTC linkers and presented large cavities and high chemical stability, as support material.[92] The detachable formate anions on the SBUs of the MOF were substituted with the carboxylate groups of the EDTA molecules to produce MOF-808-EDTA. Given the five remaining coordination sites of EDTA, MOF-808-EDTA presented excellent performance (>99%) for capturing a wide range of heavy metal ions, such as La^{3+}, Hg^{2+}, and Pb^{2+} from polluted water sources.

4. Conclusions

Owing to the modular properties of MOFs attributed to the diverse combination of inorganic species and organic linkers, many researches have focused on synthesising new structures for new functions. To overcome the limits of conventional direct synthesis, the PSM approach led to facile methods for producing desired materials. In this review, we provided recent representative examples of using the PSM approach on the SBUs of MOFs and divided the synthesis strategies into four categories: substitution of cations, redox reactions of metal centres, generation of defects, and incorporation of new species in the SBUs of MOFs. In addition, we discussed the modulation of the MOF functions owing to these simple alteration strategies as well as some interesting applications induced using the PSM approach on SBUs, such as sorption, separation, catalysis including detoxification, electron conductivity, and sensing. Unprecedented MOFs, which could not be obtained using conventional synthesis methods could be readily constructed *via* the PSM alteration of SBUs; moreover, small alterations of SBUs significantly affected the properties of the entire MOF. These simple but powerful tools present great potential for constructing MOFs for applications that have not been widely investigated yet. Moreover, it is believed that more breakthrough applications for MOFs will be uncovered in the future.

Conflicts of interest

There are no conflicts to declare.

Acknowledgements

This work was supported by the National Research Foundation of Korea (NRF) Grant funded by the Ministry of Science and ICP (No. NRF-2016R1A5A1009405, NRF-2017R1A2B4008757, and NRF-2019R1A6A3A01096867).

References

1 S. R. Batten, N. R. Champness, X.-M. Chen, J. Garcia-Martinez, S. Kitagawa, L. Öhrström, M. O'Keeffe, M. P. Suh and J. Reedijk, *CrystEngComm*, 2012, **14**, 3001–3004.
2 H. Furukawa, K. E. Cordova, M. O'Keeffe and O. M. Yaghi, *Science*, 2013, **341**, 1230444.
3 K. E. Cordova and O. M. Yaghi, *Mater. Chem. Front.*, 2017, **1**, 1304–1309.
4 F.-L. Li, Q. Shao, X. Huang and J.-P. Lang, *Angew. Chem., Int. Ed.*, 2018, **57**, 1888–1892.
5 F.-L. Li, P. Wang, X. Huang, D. J. Young, H.-F. Wang, P. Braunstein and J.-P. Lang, *Angew. Chem.*, 2019, **131**, 7125–7130.
6 A. Schoedel, M. Li, D. Li, M. O'Keeffe and O. M. Yaghi, *Chem. Rev.*, 2016, **116**, 12466–12535.
7 B. F. Hoskins and R. Robson, *J. Am. Chem. Soc.*, 1990, **112**, 1546–1554.
8 B. F. Abrahams, B. F. Hoskins, D. M. Michail and R. Robson, *Nature*, 1994, **369**, 727–729.
9 S. Subramanian and M. J. Zaworotko, *Angew. Chem., Int. Ed. Engl.*, 1995, **34**, 2127–2129.
10 O. M. Yaghi and H. Li, *J. Am. Chem. Soc.*, 1995, **117**, 10401–10402.
11 M. J. Kalmutzki, N. Hanikel and O. M. Yaghi, *Sci. Adv.*, 2018, **4**, eaat9180.
12 Z. Wang and S. M. Cohen, *Chem. Soc. Rev.*, 2009, **38**, 1315–1329.
13 L. Sarkisov, R. L. Martin, M. Haranczyk and B. Smit, *J. Am. Chem. Soc.*, 2014, **136**, 2228–2231.
14 J. H. Lee, S. Jeoung, Y. G. Chung and H. R. Moon, *Coord. Chem. Rev.*, 2019, **389**, 161–188.
15 L. Wang, C. Wang, Y. Sun, K. Shi, S. Deng and H. Lu, *Mater. Chem. Phys.*, 2016, **175**, 138–145.
16 P. Horcajada, S. Surblé, C. Serre, D.-Y. Hong, Y.-K. Seo, J.-S. Chang, J.-M. Grenèche, I. Margiolaki and G. Férey, *Chem. Commun.*, 2007, 2820–2822, DOI: 10.1039/B704325B.
17 J. H. Cavka, S. Jakobsen, U. Olsbye, N. Guillou, C. Lamberti, S. Bordiga and K. P. Lillerud, *J. Am. Chem. Soc.*, 2008, **130**, 13850–13851.
18 M. Dan-Hardi, C. Serre, T. Frot, L. Rozes, G. Maurin, C. Sanchez and G. Férey, *J. Am. Chem. Soc.*, 2009, **131**, 10857–10859.
19 J. Gao, J. Miao, P.-Z. Li, W. Y. Teng, L. Yang, Y. Zhao, B. Liu and Q. Zhang, *Chem. Commun.*, 2014, **50**, 3786–3788.
20 S. M. Cohen, *Chem. Rev.*, 2012, **112**, 970–1000.
21 V. M. Goldschmidt, *J. Chem. Soc.*, 1937, 655–673.
22 K. S. Hagen, D. W. Stephan and R. H. Holm, *Inorg. Chem.*, 1982, **21**, 3928–3936.
23 H. Li and J. D. Otvos, *Biochemistry*, 1996, **35**, 13929–13936.
24 A. Putnis, *Mineral. Mag.*, 2002, **66**, 689–708.
25 V. Autissier and R. A. Henderson, *Inorg. Chem.*, 2008, **47**, 6393–6403.
26 J. M. Pietryga, D. J. Werder, D. J. Williams, J. L. Casson, R. D. Schaller, V. I. Klimov and J. A. Hollingsworth, *J. Am. Chem. Soc.*, 2008, **130**, 4879–4885.

27 J. M. Luther, P. K. Jain, T. Ewers and A. P. Alivisatos, *Nat. Mater.*, 2011, **10**, 361.
28 K. C. Misra, *Introduction to geochemistry : principles and applications*, Wiley-Blackwell, Chichester, West Sussex, Hoboken, NJ, 2012.
29 J. B. Rivest and P. K. Jain, *Chem. Soc. Rev.*, 2013, **42**, 89–96.
30 D. J. Tranchemontagne, J. L. Mendoza-Cortés, M. O'Keeffe and O. M. Yaghi, *Chem. Soc. Rev.*, 2009, **38**, 1257–1283.
31 P. Deria, J. E. Mondloch, O. Karagiaridi, W. Bury, J. T. Hupp and O. K. Farha, *Chem. Soc. Rev.*, 2014, **43**, 5896–5912.
32 H. Wang, W. Meng, J. Wu, J. Ding, H. Hou and Y. Fan, *Coord. Chem. Rev.*, 2016, **307**, 130–146.
33 R. E. Morris and L. Brammer, *Chem. Soc. Rev.*, 2017, **46**, 5444–5462.
34 J. Ren, M. Ledwaba, N. M. Musyoka, H. W. Langmi, M. Mathe, S. Liao and W. Pang, *Coord. Chem. Rev.*, 2017, **349**, 169–197.
35 Z. Yin, S. Wan, J. Yang, M. Kurmoo and M.-H. Zeng, *Coord. Chem. Rev.*, 2019, **378**, 500–512.
36 C. K. Brozek and M. Dincă, *Chem. Soc. Rev.*, 2014, **43**, 5456–5467.
37 Z. Fang, B. Bueken, D. E. De Vos and R. A. Fischer, *Angew. Chem., Int. Ed.*, 2015, **54**, 7234–7254.
38 S. Dissegna, K. Epp, W. R. Heinz, G. Kieslich and R. A. Fischer, *Adv. Mater.*, 2018, **30**, 1704501.
39 M. Dincă and J. R. Long, *J. Am. Chem. Soc.*, 2007, **129**, 11172–11176.
40 H. J. Choi and M. P. Suh, *J. Am. Chem. Soc.*, 2004, **126**, 15844–15851.
41 T.-F. Liu, L. Zou, D. Feng, Y.-P. Chen, S. Fordham, X. Wang, Y. Liu and H.-C. Zhou, *J. Am. Chem. Soc.*, 2014, **136**, 7813–7816.
42 D. Song, J. Bae, H. Ji, M.-B. Kim, Y.-S. Bae, K. S. Park, D. Moon and N. C. Jeong, *J. Am. Chem. Soc.*, 2019, **141**, 7853–7864.
43 P.-Q. Liao, X.-Y. Li, J. Bai, C.-T. He, D.-D. Zhou, W.-X. Zhang, J.-P. Zhang and X.-M. Chen, *Chem. – Eur. J.*, 2014, **20**, 11303–11307.
44 H. R. Moon, J. H. Kim and M. P. Suh, *Angew. Chem., Int. Ed.*, 2005, **44**, 1261–1265.
45 S.-C. Qi, X.-Y. Qian, Q.-X. He, K.-J. Miao, Y. Jiang, P. Tan, X.-Q. Liu and L.-B. Sun, *Angew. Chem.*, 2019, **58**, 10104–10109.
46 Y.-G. Huang, B. Mu, P. M. Schoenecker, C. G. Carson, J. R. Karra, Y. Cai and K. S. Walton, *Angew. Chem., Int. Ed.*, 2011, **50**, 436–440.
47 C. Zhang, M. Wang, L. Liu, X. Yang and X. Xu, *Electrochem. Commun.*, 2013, **33**, 131–134.
48 H. Leclerc, T. Devic, S. Devautour-Vinot, P. Bazin, N. Audebrand, G. Férey, M. Daturi, A. Vimont and G. Clet, *J. Phys. Chem. C*, 2011, **115**, 19828–19840.
49 Z. Lu, H. G. W. Godfrey, I. da Silva, Y. Cheng, M. Savage, F. Tuna, E. J. L. McInnes, S. J. Teat, K. J. Gagnon, M. D. Frogley, P. Manuel, S. Rudić, A. J. Ramirez-Cuesta, T. L. Easun, S. Yang and M. Schröder, *Nat. Commun.*, 2017, **8**, 14212.
50 Y. Xiong, S. Chen, F. Ye, L. Su, C. Zhang, S. Shen and S. Zhao, *Chem. Commun.*, 2015, **51**, 4635–4638.
51 M. Märcz, R. E. Johnsen, P. D. C. Dietzel and H. Fjellvåg, *Microporous Mesoporous Mater.*, 2012, **157**, 62–74.
52 J. W. Yoon, Y.-K. Seo, Y. K. Hwang, J.-S. Chang, H. Leclerc, S. Wuttke, P. Bazin, A. Vimont, M. Daturi, E. Bloch, P. L. Llewellyn, C. Serre, P. Horcajada, J.-M. Grenèche, A. E. Rodrigues and G. Férey, *Angew. Chem., Int. Ed.*, 2010, **49**, 5949–5952.
53 H. Irving and R. J. P. Williams, *J. Chem. Soc.*, 1953, 3192–3210.
54 K. Li and D. Xue, *J. Phys. Chem. A*, 2006, **110**, 11332–11337.
55 M. Kim, J. F. Cahill, H. Fei, K. A. Prather and S. M. Cohen, *J. Am. Chem. Soc.*, 2012, **134**, 18082–18088.
56 C. K. Brozek and M. Dincă, *J. Am. Chem. Soc.*, 2013, **135**, 12886–12891.
57 J. Tu, X. Zeng, F. Xu, X. Wu, Y. Tian, X. Hou and Z. Long, *Chem. Commun.*, 2017, **53**, 3361–3364.
58 G. Férey and C. Serre, *Chem. Soc. Rev.*, 2009, **38**, 1380–1399.
59 L. J. Murray, M. Dinca, J. Yano, S. Chavan, S. Bordiga, C. M. Brown and J. R. Long, *J. Am. Chem. Soc.*, 2010, **132**, 7856–7857.
60 A. Phan, C. J. Doonan, F. J. Uribe-Romo, C. B. Knobler, M. O'Keeffe and O. M. Yaghi, *Acc. Chem. Res.*, 2010, **43**, 58–67.
61 D. Feng, Z.-Y. Gu, J.-R. Li, H.-L. Jiang, Z. Wei and H.-C. Zhou, *Angew. Chem., Int. Ed.*, 2012, **51**, 10307–10310.
62 H.-L. Jiang, D. Feng, T.-F. Liu, J.-R. Li and H.-C. Zhou, *J. Am. Chem. Soc.*, 2012, **134**, 14690–14693.
63 P. Capper, *Bulk Crystal Growth of Electronic, Optical and Optoelectronic Materials*, Wiley, New York, 2005.
64 B. Tu, Q. Pang, D. Wu, Y. Song, L. Weng and Q. Li, *J. Am. Chem. Soc.*, 2014, **136**, 14465–14471.
65 S. Gadipelli and Z. Guo, *Chem. Mater.*, 2014, **26**, 6333–6338.
66 B. Bueken, N. Van Velthoven, A. Krajnc, S. Smolders, F. Taulelle, C. Mellot-Draznieks, G. Mali, T. D. Bennett and D. De Vos, *Chem. Mater.*, 2017, **29**, 10478–10486.
67 G. C. Shearer, S. Chavan, J. Ethiraj, J. G. Vitillo, S. Svelle, U. Olsbye, C. Lamberti, S. Bordiga and K. P. Lillerud, *Chem. Mater.*, 2014, **26**, 4068–4071.
68 F. Vermoortele, R. Ameloot, L. Alaerts, R. Matthessen, B. Carlier, E. V. R. Fernandez, J. Gascon, F. Kapteijn and D. E. De Vos, *J. Mater. Chem.*, 2012, **22**, 10313–10321.
69 G.-Y. Jeong, A. K. Singh, M.-G. Kim, K.-W. Gyak, U. Ryu, K. M. Choi and D.-P. Kim, *Nat. Commun.*, 2018, **9**, 3968.
70 T. M. McDonald, W. R. Lee, J. A. Mason, B. M. Wiers, C. S. Hong and J. R. Long, *J. Am. Chem. Soc.*, 2012, **134**, 7056–7065.
71 Y.-S. Wei, M. Zhang, P.-Q. Liao, R.-B. Lin, T.-Y. Li, G. Shao, J.-P. Zhang and X.-M. Chen, *Nat. Commun.*, 2015, **6**, 8348.
72 P. Deria, J. E. Mondloch, E. Tylianakis, P. Ghosh, W. Bury, R. Q. Snurr, J. T. Hupp and O. K. Farha, *J. Am. Chem. Soc.*, 2013, **135**, 16801–16804.

73 S. Yuan, W. Lu, Y.-P. Chen, Q. Zhang, T.-F. Liu, D. Feng, X. Wang, J. Qin and H.-C. Zhou, *J. Am. Chem. Soc.*, 2015, **137**, 3177–3180.
74 S. Yuan, Y.-P. Chen, J.-S. Qin, W. Lu, L. Zou, Q. Zhang, X. Wang, X. Sun and H.-C. Zhou, *J. Am. Chem. Soc.*, 2016, **138**, 8912–8919.
75 M. Meilikhov, K. Yusenko and R. A. Fischer, *J. Am. Chem. Soc.*, 2009, **131**, 9644–9645.
76 D. Yang, S. O. Odoh, T. C. Wang, O. K. Farha, J. T. Hupp, C. J. Cramer, L. Gagliardi and B. C. Gates, *J. Am. Chem. Soc.*, 2015, **137**, 7391–7396.
77 Z. Zhang, L. Wojtas, M. Eddaoudi and M. J. Zaworotko, *J. Am. Chem. Soc.*, 2013, **135**, 5982–5985.
78 T. M. McDonald, J. A. Mason, X. Kong, E. D. Bloch, D. Gygi, A. Dani, V. Crocellà, F. Giordanino, S. O. Odoh, W. S. Drisdell, B. Vlaisavljevich, A. L. Dzubak, R. Poloni, S. K. Schnell, N. Planas, K. Lee, T. Pascal, L. F. Wan, D. Prendergast, J. B. Neaton, B. Smit, J. B. Kortright, L. Gagliardi, S. Bordiga, J. A. Reimer and J. R. Long, *Nature*, 2015, **519**, 303.
79 R. L. Siegelman, P. J. Milner, A. C. Forse, J.-H. Lee, K. A. Colwell, J. B. Neaton, J. A. Reimer, S. C. Weston and J. R. Long, *J. Am. Chem. Soc.*, 2019, **141**, 13171–13186.
80 R.-B. Lin, L. Li, H.-L. Zhou, H. Wu, C. He, S. Li, R. Krishna, J. Li, W. Zhou and B. Chen, *Nat. Mater.*, 2018, **17**, 1128–1133.
81 J. J. M. Beenakker, V. D. Borman and S. Y. Krylov, *Chem. Phys. Lett.*, 1995, **232**, 379–382.
82 H. Oh, K. S. Park, S. B. Kalidindi, R. A. Fischer and M. Hirscher, *J. Mater. Chem. A*, 2013, **1**, 3244–3248.
83 S. A. FitzGerald, C. J. Pierce, J. L. C. Rowsell, E. D. Bloch and J. A. Mason, *J. Am. Chem. Soc.*, 2013, **135**, 9458–9464.
84 J. Y. Kim, H. Oh and H. R. Moon, *Adv. Mater.*, 2019, **31**, 1970147.
85 I. Weinrauch, I. Savchenko, D. Denysenko, S. M. Souliou, H. H. Kim, M. Le Tacon, L. L. Daemen, Y. Cheng, A. Mavrandonakis, A. J. Ramirez-Cuesta, D. Volkmer, G. Schütz, M. Hirscher and T. Heine, *Nat. Commun.*, 2017, **8**, 14496.
86 D. Denysenko, M. Grzywa, J. Jelic, K. Reuter and D. Volkmer, *Angew. Chem., Int. Ed.*, 2014, **53**, 5832–5836.
87 J. Y. Kim, R. Balderas-Xicohténcatl, L. Zhang, S. G. Kang, M. Hirscher, H. Oh and H. R. Moon, *J. Am. Chem. Soc.*, 2017, **139**, 15135–15141.
88 A. M. Abdel-Mageed, B. Rungtaweevoranit, M. Parlinska-Wojtan, X. Pei, O. M. Yaghi and R. J. Behm, *J. Am. Chem. Soc.*, 2019, **141**, 5201–5210.
89 J. Zheng, J. Ye, M. A. Ortuño, J. L. Fulton, O. Y. Gutiérrez, D. M. Camaioni, R. K. Motkuri, Z. Li, T. E. Webber, B. L. Mehdi, N. D. Browning, R. L. Penn, O. K. Farha, J. T. Hupp, D. G. Truhlar, C. J. Cramer and J. A. Lercher, *J. Am. Chem. Soc.*, 2019, **141**, 9292–9304.
90 E. López-Maya, C. Montoro, L. M. Rodríguez-Albelo, S. D. Aznar Cervantes, A. A. Lozano-Pérez, J. L. Cenís, E. Barea and J. A. R. Navarro, *Angew. Chem., Int. Ed.*, 2015, **54**, 6790–6794.
91 R. Gil-San-Millan, E. López-Maya, A. E. Platero-Prats, V. Torres-Pérez, P. Delgado, A. W. Augustyniak, M. K. Kim, H. W. Lee, S. G. Ryu and J. A. R. Navarro, *J. Am. Chem. Soc.*, 2019, **141**, 11801–11805.
92 P. Sippel, D. Denysenko, A. Loidl, P. Lunkenheimer, G. Sastre and D. Volkmer, *Adv. Funct. Mater.*, 2014, **24**, 3885–3896.
93 L. Sun, M. G. Campbell and M. Dincă, *Angew. Chem., Int. Ed.*, 2016, **55**, 3566–3579.
94 A. A. Talin, A. Centrone, A. C. Ford, M. E. Foster, V. Stavila, P. Haney, R. A. Kinney, V. Szalai, F. El Gabaly, H. P. Yoon, F. Léonard and M. D. Allendorf, *Science*, 2014, **343**, 66.
95 A.-L. Li, Q. Gao, J. Xu and X.-H. Bu, *Coord. Chem. Rev.*, 2017, **344**, 54–82.
96 N. C. Jeong, B. Samanta, C. Y. Lee, O. K. Farha and J. T. Hupp, *J. Am. Chem. Soc.*, 2012, **134**, 51–54.
97 X. Meng, H.-N. Wang, L.-S. Wang, Y.-H. Zou and Z.-Y. Zhou, *CrystEngComm*, 2019, **21**, 3146–3150.
98 C.-X. Yang, H.-B. Ren and X.-P. Yan, *Anal. Chem.*, 2013, **85**, 7441–7446.
99 Y. Peng, H. Huang, Y. Zhang, C. Kang, S. Chen, L. Song, D. Liu and C. Zhong, *Nat. Commun.*, 2018, **9**, 187.
100 P. J. Milner, R. L. Siegelman, A. C. Forse, M. I. Gonzalez, T. Runčevski, J. D. Martell, J. A. Reimer and J. R. Long, *J. Am. Chem. Soc.*, 2017, **139**, 13541–13553.
101 K. Son, J. Y. Kim, G. Schütz, S. G. Kang, H. R. Moon and H. Oh, *Inorg. Chem.*, 2019, **58**, 8895–8899.
102 M. J. Ingleson, R. Heck, J. A. Gould and M. J. Rosseinsky, *Inorg. Chem.*, 2009, **48**, 9986–9988.
103 M. Banerjee, S. Das, M. Yoon, H. J. Choi, M. H. Hyun, S. M. Park, G. Seo and K. Kim, *J. Am. Chem. Soc.*, 2009, **131**, 7524–7525.
104 Y. K. Hwang, D.-Y. Hong, J.-S. Chang, S. H. Jhung, Y.-K. Seo, J. Kim, A. Vimont, M. Daturi, C. Serre and G. Férey, *Angew. Chem., Int. Ed.*, 2008, **47**, 4144–4148.
105 J. M. Fernández-Morales, L. A. Lozano, E. Castillejos-López, I. Rodríguez-Ramos, A. Guerrero-Ruiz and J. M. Zamaro, *Microporous Mesoporous Mater.*, 2019, **290**, 109686.
106 D. Sun, P. R. Adiyala, S.-J. Yim and D.-P. Kim, *Angew. Chem.*, 2019, **131**, 7483–7487.
107 A. Atilgan, T. Islamoglu, A. J. Howarth, J. T. Hupp and O. K. Farha, *ACS Appl. Mater. Interfaces*, 2017, **9**, 24555–24560.
108 P. Deria, Y. G. Chung, R. Q. Snurr, J. T. Hupp and O. K. Farha, *Chem. Sci.*, 2015, **6**, 5172–5176.
109 P. Liu, E. Redekop, X. Gao, W.-C. Liu, U. Olsbye and G. A. Somorjai, *J. Am. Chem. Soc.*, 2019, **141**, 11557–11564.
110 C. A. Trickett, T. M. O. Popp, J. Su, C. Yan, J. Weisberg, A. Huq, P. Urban, J. Jiang, M. J. Kalmutzki, Q. Liu, J. Baek, M. P. Head-Gordon, G. A. Somorjai, J. A. Reimer and O. M. Yaghi, *Nat. Chem.*, 2019, **11**, 170–176.

111 P. Ji, X. Feng, P. Oliveres, Z. Li, A. Murakami, C. Wang and W. Lin, *J. Am. Chem. Soc.*, 2019, **141**, 14878–14888.
112 J. E. Mondloch, W. Bury, D. Fairen-Jimenez, S. Kwon, E. J. DeMarco, M. H. Weston, A. A. Sarjeant, S. T. Nguyen, P. C. Stair, R. Q. Snurr, O. K. Farha and J. T. Hupp, *J. Am. Chem. Soc.*, 2013, **135**, 10294–10297.
113 M. Rimoldi, A. Nakamura, N. A. Vermeulen, J. J. Henkelis, A. K. Blackburn, J. T. Hupp, J. F. Stoddart and O. K. Farha, *Chem. Sci.*, 2016, **7**, 4980–4984.
114 I. S. Kim, J. Borycz, A. E. Platero-Prats, S. Tussupbayev, T. C. Wang, O. K. Farha, J. T. Hupp, L. Gagliardi, K. W. Chapman, C. J. Cramer and A. B. F. Martinson, *Chem. Mater.*, 2015, **27**, 4772–4778.
115 X. Wang, X. Zhang, P. Li, K.-i. Otake, Y. Cui, J. Lyu, M. D. Krzyaniak, Y. Zhang, Z. Li, J. Liu, C. T. Buru, T. Islamoglu, M. R. Wasielewski, Z. Li and O. K. Farha, *J. Am. Chem. Soc.*, 2019, **141**, 8306–8314.
116 J. G. Santaclara, A. I. Olivos-Suarez, A. Gonzalez-Nelson, D. Osadchii, M. A. Nasalevich, M. A. van der Veen, F. Kapteijn, A. M. Sheveleva, S. L. Veber, M. V. Fedin, A. T. Murray, C. H. Hendon, A. Walsh and J. Gascon, *Chem. Mater.*, 2017, **29**, 8963–8967.
117 K. Manna, P. Ji, Z. Lin, F. X. Greene, A. Urban, N. C. Thacker and W. Lin, *Nat. Commun.*, 2016, **7**, 12610.
118 B. An, Z. Li, Y. Song, J. Zhang, L. Zeng, C. Wang and W. Lin, *Nat. Catal.*, 2019, **2**, 709–717.
119 P. Ji, K. Manna, Z. Lin, A. Urban, F. X. Greene, G. Lan and W. Lin, *J. Am. Chem. Soc.*, 2016, **138**, 12234–12242.
120 P. Ji, Y. Song, T. Drake, S. S. Veroneau, Z. Lin, X. Pan and W. Lin, *J. Am. Chem. Soc.*, 2018, **140**, 433–440.
121 K. Manna, P. Ji, F. X. Greene and W. Lin, *J. Am. Chem. Soc.*, 2016, **138**, 7488–7491.
122 P. Ji, K. Manna, Z. Lin, X. Feng, A. Urban, Y. Song and W. Lin, *J. Am. Chem. Soc.*, 2017, **139**, 7004–7011.
123 S. Yuan, Y.-P. Chen, J. Qin, W. Lu, X. Wang, Q. Zhang, M. Bosch, T.-F. Liu, X. Lian and H.-C. Zhou, *Angew. Chem., Int. Ed.*, 2015, **54**, 14696–14700.
124 N. Van Velthoven, S. Waitschat, S. M. Chavan, P. Liu, S. Smolders, J. Vercammen, B. Bueken, S. Bals, K. P. Lillerud, N. Stock and D. E. De Vos, *Chem. Sci.*, 2019, **10**, 3616–3622.
125 K.-i. Otake, Y. Cui, C. T. Buru, Z. Li, J. T. Hupp and O. K. Farha, *J. Am. Chem. Soc.*, 2018, **140**, 8652–8656.
126 Y. Song, Z. Li, P. Ji, M. Kaufmann, X. Feng, J. S. Chen, C. Wang and W. Lin, *ACS Catal.*, 2019, **9**, 1578–1583.